Ocean Sci. Discuss., 10, 435–472, 2013
www.ocean-sci-discuss.net/10/435/2013/
doi:10.5194/osd-10-435-2013

Ocean Science
Discussions
Open Access

Tidal variability of the motion in the Strait of Otranto

L. Ursella, V. Kovačević, and M. Gačić

Istituto Nazionale di Oceanografia e di Geofisica Sperimentale (OGS), B.go Grotta Gigante 42/c, 34010 Sgonico (TS), Italy

Received: 24 January 2013 – Accepted: 10 February 2013 – Published: 5 March 2013

Correspondence to: L. Ursella (lursella@ogs.trieste.it)

Published by Copernicus Publications on behalf of the European Geosciences Union.

Abstract

Various current data, collected in the Strait of Otranto during the period 1994–2007, have been analysed with the aim of describing the characteristics of the tidal motions and their contribution to the total flow variance. The principal tidal constituents in the area were the semi-diurnal (M2) and the diurnal (K1), with the latter one predominant. The total flow was, in general, more energetic along the flanks than in the middle of the Strait. Specifically, it was most energetic over the western shelf and in the upper layer along the eastern flank. In spite of the generally low velocities (a few $cm\,s^{-1}$) of the principal tidal constituents, the tidal variance has a pattern similar to that of the total flow variance, that is, it was large over the western shelf and low in the middle. The proportion of non-tidal (comprising the inertial and sub-inertial low-frequency bands) to tidal flow variances was quite variable in both time and space. The contribution of the low-frequency motions predominated over the tidal and inertial ones in the eastern portion of the strait during the major part of the year, particularly in the upper and intermediate layers. In the deep, near-bottom, layer the variance was evenly distributed between the low frequency, diurnal and semi-diurnal bands. A prominent exception was observed near the western shelf break during the summer season when the contribution of the tidal signal alone to the total variance reached 77 %. This high contribution was mainly due to the intensification of the diurnal signal at that location in the proximity of both the surface and bottom layers (velocities of about $10\,cm\,s^{-1}$). Local wind and sea level data were analysed and compared with the flow to find the possible origin of this diurnal intensification. Having excluded the sea-breeze impact on the intensification of the diurnal tidal signal, the most likely cause remains the generation of the topographically trapped internal waves and the diurnal resonance in the tidal response. These waves were sometimes generated by the barotropic tidal signal in the presence of summer stratification. The effect was seen only in the presence of the topographic slope change. This phenomenon may stimulate the diapycnal mixing during the stratified season and enhance ventilation of the near-bottom layers.

OSD
10, 435–472, 2013

1 Introduction

The notion of tidal variability was historically better described from the measurements of the sea level than from measurements of the sea currents. The simplicity, low cost and easy maintenance of the tide gauges at the coast compared to current-meter moorings are the main reason for this historical discrepancy. Therefore, the study of the tidal oscillations of the sea level in the Adriatic Sea has a long and rich history, and it is principally focused on the diurnal and semi-diurnal bands.

Experimental studies dealing with the sea level were conducted by Polli (1960), Mosetti and Manca (1972), Buljan and Zore-Armanda (1976) and Orlić (2001). The tidal motion in the Adriatic is induced by the Mediterranean Sea tide, and co-oscillates with it. Polli (1960) drew charts of the cotidal lines and lines of equal phases for the surface elevation of the entire Adriatic Sea. He showed that the semi-diurnal tide has a sea-level amphidromic point located off Ancona (at about 14.5° E, 43.5° N), and that there is no amphydromic point for the diurnal tide. Theoretical studies (Taylor, 1921; Hendershot and Speranza, 1971) explained that semi-diurnal tide (the principal one in the basin) propagates as a Kelvin wave entering from the Strait of Otranto, travelling to the north along the eastern coast, reflecting at the basin's end and descending the Adriatic along the western coast. As a result, an amphidromic point for the currents is positioned off the Gargano promontory (at around 16° E, 42° N), that is, south of the one for the sea level. The maxima in the current tide therefore correspond to minima in the sea level (Hendershott and Speranza, 1971). From numerical model studies, Malačič et al. (2000) explained the dynamics of semi-diurnal and diurnal tides in the northern Adriatic with a general theory of gravity and topographic waves. Thus, the M2 tide is well represented by a Kelvin wave that propagates along the basin, as gravity dominates, while K1 is well approximated by a continental shelf wave propagating across the basin as topography dominates. In addition to the above-mentioned papers there has been a considerable amount of other theoretical and observational research on tides; results and findings up to 2001 are summarized by Cushman-Roisin et al. (2001).

OSD
10, 435–472, 2013

Current-meter measurements of sufficient duration to determine the tidal flow constituents have been something of a challenge all over the Adriatic Sea due to costs and instrument losses caused mainly by heavy fishery activities. Tidal currents derived from current-meter measurements as found in the literature refer predominantly to the northern Adriatic Sea. In particular, studies in the channels along the eastern coast (references in Cushman-Roisin et al., 2001) showed tidal flow ranges between 1 and 10 cm s^{-1}. Tidal characteristics of the surface current along the northern Italian coast were studied by Budillon et al. (2002), Kovačević et al. (2004) and Chavanne et al. (2007), while the detailed vertical pattern of the tidal flow throughout the water column was examined in the northernmost part of the basin by Book et al. (2009) and in the central Adriatic by Martin et al. (2009). All these studies show that the values of the semi-major axes are a few cm s^{-1} (M2 was mostly between 5 and 7 cm s^{-1} and K1 between 2 and 4 cm s^{-1}).

However, a basin-wide survey in 1995 by a Vessel Mounted Acoustic Doppler Current Profiler (VM-ADCP) made possible a description of the distribution of the M2 tidal current ellipses for a wider area of the Adriatic basin (Ursella and Gačić, 2001).

Recent numerical modelling studies (Cushman-Roisin and Naimie, 2002; Janeković et al., 2003; Janeković and Kuzmić, 2005) are based on 3-D, high resolution, numerical models. In particular, Janeković and Kuzmić (2005) obtained satisfactory results, as demonstrated from the comparison of numerical data with the observed sea levels from several tide gauges around the coast, and with some sporadic current-meter data from some locations in the northern Adriatic Sea.

On the other hand, studies based on detailed observations of tidal currents across the Strait of Otranto have not been made before. From some sporadic and short-lasting measurements that were conducted in the eighties and nineties in that area (i.e., Michelato and Kovačević, 1991; Leder et al., 1992; Ferentinos and Castanos, 1988) it turned out that the flow has prominent diurnal and inertial fluctuations. In addition, the most recent studies based on the current measurements in the southern Adriatic found

OSD
10, 435–472, 2013

evidence of fortnightly oscillations of the flow over the shelf break in phase with Mf tide (Vilibić et al., 2010).

In numerical studies the Strait has been taken into account either as an open boundary of the Adriatic Sea (i.e, Janeković and Kuzmić, 2005) or as a part of the wider area. A tidal model for the barotropic M2 for the whole Mediterranean was developed by Lozano and Candela (1995). While the results agreed well over most of the Adriatic with the findings of Ursella and Gačić (2001), a full comparison for the Strait of Otranto was not possible because of the lack of measurements.

The long-term currents (for more than a month) collected in the Strait of Otranto intermittently from the 1990s until 2007 build a unique data set for studying the flow characteristics in the area, primarily as the exchange of water and biogeochemical properties between the Adriatic and Ionian Sea. In the past studies the emphasis was on the low frequency (with periods of about a week), and seasonal flow and transport variability (Gačić et al., 1996; Vetrano et al., 1999, Kovačević et al., 1999; Ursella et al., 2011, 2012, Yari et al., 2012) or on the inter-annual variability related to the processes of the dense water formation (Manca et al., 2002). The interest in the transport rate and its seasonal and inter-annual variability did not include a thorough and exhaustive analysis of the flow in the diurnal and semi-diurnal tidal frequency band. We used data collected along the mooring arrays in the Strait of Otranto (Fig. 1), within the framework of the Mediterranean Targeted Project (MTP) – OTRANTO, Otranto Gap EXperiment (OGEX), MTP II-MATER (MAss Transfer and Ecosystem Response) and VECTOR (VulnErabilità delle Coste e degli ecosistemi marini italiani ai cambiamenti climaTici e loro ruolO nei cicli del caRbonio mediterraneo) projects. We also addressed the phenomenon of baroclinic diurnal tide intensification in the deep layers over the western shelf edge.

A number of studies on baroclinic internal tide generation in the presence of abrupt topographic features are found in the literature (Beckenbach and Terril, 2008, and references therein). In particular, it has been found that interaction between barotropic tidal currents and topography generates a baroclinic internal tide; the diurnal one resembles

OSD
10, 435–472, 2013

the first baroclinic mode which is topographically distorted, amplified and polarized in the near-bottom layer. These effects were not observed in the semi-diurnal response.

This paper is structured as follows: data and methods are presented in Sect. 2, description of the spatial and seasonal variability of the tidal signal is given in Sect. 3, detailed considerations of the bottom layer characteristics are exposed in Sect. 4, intensification of the diurnal tide at the western shelf-break and slope is discussed in Sect. 5 and, finally, Sect. 6 contains concluding remarks.

2 Data and methods

2.1 Mooring arrangement and deployment

The current data set originates from several moorings that were deployed in the Strait of Otranto (Fig. 1), during three long-term observations. The first one was the OTRANTO/OGEX project, which spanned the time interval from February 1994 to November 1995 (Fig. 2a). The second set of observations was in the period from March 1997 to July 1999 (Fig. 2b) in the framework of the MTP II-MATER project, and the third was in the period from November 2006 to April 2007 (Fig. 2c) in the framework of the VECTOR project.

Some findings from the OTRANTO/OGEX project current data set used in this study were reported by Kovačević et al. (1999). Briefly, currents were measured at six stations: M1, M2, M3, M4, M5 and M6 (Fig. 1b, c). The stations were positioned along an east–west transect in the southernmost part of the Adriatic Sea at 39°50′ N. Typically, the currents were measured in three layers, the surface layer (28–42 m depth interval), the intermediate layer (300–330 m depth) and near-bottom layers, a few tens of meters above the sea bed. There were some gaps in the data set due to instrument and battery malfunctioning. The moorings at locations M1 and M2 on the western side included two current meters, while moorings in the central and western parts at locations M3, M5 and M6 included three current meters (Fig. 1). Four types of self-recording

OSD
10, 435–472, 2013

current meters were used on the moorings. The NBA-DNC-2B with rotor and EG&G SMART acoustic current meters recorded a mean speed and instantaneous direction every 20 and 10 min respectively. The Aanderaa RCM7 current meter recorded an hourly current vector averaged from 50 samples taken every 72 s. At M4 only, apart from the bottom current meter, an RDI ADCP operating at 75 KHz was deployed at about 430 m below the sea surface, looking upward to measure the currents in the water column in 8-m bins. Because of the high vertical correlation of the ADCP current data, the time series from just the uppermost and the lowermost cells (near-surface layer and mid-depth) were considered representative of the upper and intermediate layers, respectively. All the moorings were recovered almost every 3 months and redeployed after maintenance. The accuracy of the aforementioned instruments for measuring the speed and direction are 1 cm s^{-1} and 3–7.5°, respectively. The data subset chosen for the present purpose is from the time interval November 1994–November 1995 (Fig. 2a).

MATER moorings were equipped with RDI BB ADCPs which recorded the deep currents above the seabed, within about 160 m at stations O1 and O2 and about 50 m at O3, with a vertical resolution of 5 m and a sampling rate of 30 min. MATER moorings were deployed five times and each data series is about 6 months long (Fig. 2b).

VECTOR moorings were equipped with: (i) an Aanderaa current-meter, 17 m above the seabed, whose sampling rate was 30 min; (ii) a conductivity–temperature SBE37 CT probe 2 m above the current meter, with a sampling rate of 15 min; and (iii) an upward-looking RDI ADCP 10 m above the CT, with a sampling interval of 15 min. The ADCP measurements covered a layer of about 100 m at station V3 and of about 80 m at V2 and V4.

A detailed description of the mooring arrangement and schedule during the MATER and VECTOR projects can be found in Ursella et al. (2012) and references therein. As the VECTOR stations V2, V3 and V4 correspond to O1, O2 and O3 in the MATER project, and stations M3 and M4 of the OTRANTO/OGEX project roughly coincide with V2 and V3 respectively (Fig. 1), a unique nomenclature is used in the following: St1 for

OSD
10, 435–472, 2013

station M1, St2 for station M2, St3 for stations M3, O1 and V2, St4 for O2 and V3, St5 for M4 and O3 for the first measurement phase, St6 for M5, O3 and V4 and, finally, St7 for M6.

2.2 Data processing

For all the analysis considered herein, each ADCP cell was treated as an independent time series and each measurement period separately analyzed. ADCP data and current-meter series were treated in the same way, using the same procedure in data analysis. Quality control was carried out, removing spikes and bad data, while the missing data within the gaps lasting for less than 6 h were linearly interpolated.

Three periods were chosen for the OTRANTO/OGEX project: P1, from December 1994 to January 1995; P2, from June to August 1995; and P3, from September to November 1995 (Fig. 2a). These three periods were considered roughly as winter, summer and autumn seasons. They were selected for the sake of the best possible time and space coverage along the Otranto section.

For the other two projects, MATER and VECTOR, only bottom-layer data were available. The periods for the analysis differ from the OTRANTO/OGEX ones, and they are simply the periods of each deployment (Fig. 2b and c). It must be kept in mind that during the first phase of MATER (A), current-meter O3 was positioned at station St5 while during the other measurement phases it was deployed at station St6 and was therefore deeper.

On the edited and interpolated data, rotary spectra were calculated for each instrument depth and period. The following different window lengths were applied: 256 points for OTRANTO/OGEX hourly data and 2048 and 4096 points for raw originally sampled MATER and VECTOR data, respectively. The overlapping period always corresponded to the window half-length. Harmonic analysis (Foreman, 1978) was applied in order to obtain tidal constituents. Harmonic analysis calculations were done using the Matlab programme t_tide (Pawlowicz et al., 2002). The method also enables calculation of the percentage of the total variance accounted for by the resolved tidal signal.

OSD
10, 435–472, 2013

For each of the selected periods, the length in time (two months, the shortest one) permits resolution of different tidal constituents within each of the two major bands (diurnal and semi-diurnal).

For the purposes of the analysis of Sect. 5 only, the periods of the OTRANTO/OGEX project are selected in a different way with respect to P1, P2 and P3.

3 Spatial and seasonal variability of the tidal signal

The data from the OTRANTO/OGEX project are the only ones that cover the entire Otranto section and were therefore used to study the vertical and horizontal variability of the tidal motion that it is discussed in this section.

As already indicated, the rotary spectral analysis and harmonic analysis of the OTRANTO/OGEX data set are ultimately limited to the three time periods P1, P2 and P3. In order to address the most salient characteristics, the results we report here are split into three groups: upper layer, intermediate layer and bottom layer.

3.1 Variance and Spectral analysis

Figure 3 summarises the variance in the three layers within each period at different moorings. The tidal signal is composed of the 35 constituents resolved by the harmonic analysis. The percentage of the predicted variance to the total one is also depicted. The percentage was always below 40 %, apart from the stratified period P2 at St2, when it reached about 60 % at the top and 77 % at the bottom, and at St7-bottom where the value was 47 %.

The upper-layer tidal analysis is based on mostly point-wise current measurements at depths varying between 28 and 42 m below the sea surface. However, it must be kept in mind that the surface current meter at St2 during period P2 was positioned at 56 m depth and was thus not really a surface one. The western flank (station St1) of the strait was characterized by the largest total variance (Fig. 3) and by the largest tidal variance

OSD
10, 435–472, 2013

as well. The central portion of the section had both total and tidal variance lower than at both flanks. The only comparison available for the nearby locations over the western shelf (St1 and St2) is for the period P1, during which the total and tidal variances decreased rapidly in the offshore direction. A significant fluctuation in the variance in time and space is due to the varying energy levels of both the tidal and the non-tidal bands. The spectral characteristics of the upper layer show that the flow variance was distributed principally among the tidal oscillations (diurnal and semi-diurnal), inertial oscillations (0.053454 cph–18.7 h period) and a long-period motion (Fig. 4). The diurnal tidal band was more energetic than the semi-diurnal one. Moreover, at the shelf break (station St2) during period P2 the diurnal one was the principal peak in the spectrum, with particularly high energy at negative frequencies (indicating a clock-wise rotation of the tidal vector). Inertial oscillations, indicated by a dominant peak at a negative frequency, were more energetic than the diurnal one except during the P2 period at the shelf break (station St2). During P1 and P3 the low-frequency band was predominant and it was more energetic at the flanks, both eastern (station St7) and western (station St1), than in the middle of the strait (Fig. 4).

The measurements in the intermediate layer were obviously carried out only in the deepest portion of the section (stations from St3 to St7). The total and tidal variances (Fig. 3) showed extremely low energetics at these intermediate depths. The spectral characteristics (not shown) indicate that low-frequency motion was the most energetic portion. Inertial oscillations were attenuated with respect to the surface layer (Fig. 4), and display values similar to those of the semi-diurnal and diurnal tides.

In the bottom layer, total variance (Fig. 3) was larger over the continental shelf (station St1), gradually diminishing in the offshore direction. The tidal contribution also diminished from the shelf toward the eastern flank. Tidal variance was exceptionally high over the shelf edge (station St2) during the stratified P2 time interval. In general the low-frequency motion (Fig. 5) was the most energetic; however, an exception to this was observed at station St2 during all the three periods when the diurnal signal dominated. In addition during P2 the semi-diurnal band was also as energetic as the

OSD
10, 435–472, 2013

low-frequency one. As for the surface, the direction of rotation was clockwise. In the central deep portion of the strait (stations St5 and St6), the low frequency dominated over the tidal and inertial ones.

In conclusion, the total variance was maximum at the westernmost two stations and at the easternmost surface one. Predicted tidal variance behaved similarly to the total variance. In addition it shows an intensification over the shelf break (St2). Moreover, the percentage of the variance due to tidal signal with respect to the total variance was maximum at the shelf break, reaching 77 % during period P2.

3.2 Harmonic analysis

The temporal and spatial variability of the tidal signal was studied by means of harmonic analysis of the OTRANTO/OGEX data sets. Three principal bands were distinguished: long-term, diurnal and semi-diurnal.

Tidal constituents MM and MFS, with frequencies of 0.0015 and 0.0028 cyc h^{-1} respectively (that is, with periods of 27.78 and 14.88 days), are grouped in the long-term tidal band. Their amplitudes were highly variable in time and space (not shown), probably due to the fact that with the harmonic analysis it was not always possible to distinguish between the astronomical tidal forcing and the non-tidal low-frequency meteorological signal with periods of about 10 days. The largest amplitudes of this signal were encountered along the western and eastern flanks, while the smallest was in the central part, resembling the pattern of the entire non-tidal variance (Fig. 3).

Figure 6 summarises the amplitudes of the semi-major axes of the diurnal and semi-diurnal tidal ellipses. The constituents that showed the largest value of the tidal ellipse semi-major axis, namely K1 (0.04178 cyc h^{-1}) and M2 (0.08051 cyc h^{-1}), were taken as representative of the corresponding band. Amplitudes of the K1 diurnal constituent were always below 6 cm s^{-1} except for at station St2, where the amplitude reached 10 and 15 cm s^{-1} in the near-surface and bottom records, respectively, during the stratified period P2. Amplitudes of the M2 constituent were always below 3 cm s^{-1}. The K1 semi-major axes of tidal ellipses were almost twice those of M2 and were thus the main tidal

OSD
10, 435–472, 2013

signal in the flow. The M2 tidal constituent had somewhat larger amplitudes along the flanks and smaller in the centre of the section. It did not show much change from P1 to P3. There was, in contrast and as already mentioned, an anomalous feature of the diurnal constituent K1: an amplification at the shelf break (station St2) just visible in the OTRANTO/OGEX summer time-series (P2 period). Unfortunately, due to the lack of measurements on the shelf, no confirmation of this characteristic was encountered either during other periods of the OTRANTO/OGEX or during the MATER and VECTOR projects. The intensification at the shelf break is described and discussed in detail in Sect. 5.

4 Detailed look into the bottom layer in the deep portion of the Strait

The data set from the MATER and VECTOR projects permits accurate description of the tides in the bottom layer. Rotary spectra (Fig. 7) show that inertial, diurnal and semi-diurnal bands were always present at all stations and during all periods. The energy of these peaks was lower at station St4 during the last MATER measurement phase (E). In particular, the diurnal constituent was always more energetic at location St3 than at other locations, where its energy could be almost as high as the low-frequency one, as during the VECTOR period. This characteristic may indicate an amplification of the diurnal tidal signal near the shelf break (see the position of St3 in Fig. 1). Moreover, no significant differences in the spectra were found between upper and lower cells at any current meter (not shown).

Total and tidal (predicted) variances are depicted in Fig. 8 as a function of depth for MATER and VECTOR data. In general the highest total variance was found at the central station St4 (see also Ursella et al., 2011), where it decreased toward the bottom. At the other two lateral moorings (St3 and St5/St6) it remained constant or increased while approaching the bottom. Tidal predicted variance was always less than 30 % of the total variance, and it was almost always highest at St3. Its contribution to the total variance at this mooring was generally larger than 15 %, except for the period E when

OSD
10, 435–472, 2013

the non-tidal, and hence the total, variance was very high. This again shows that near the shelf break the tidal signal was more important than in the deep central part of the strait. The lowest tidal contribution to the total variance was found at St4, indicating a variability in the current field due principally to non-tidal phenomena. Finally, the lowest percentages at the three stations were found during period E, when the non-tidal variability was rather strong.

Tidal semi-major axes for the two main constituents, K1 and M2, are depicted in Fig. 9 together with the orientation of the tidal ellipses. The K1 constituent was always larger than M2 and it assumed the greatest values at location St3, reaching 3 to 5 $\mathrm{cm\,s^{-1}}$ during all the periods except phase D when it was about 2 $\mathrm{cm\,s^{-1}}$. The K1 semi-major axes slightly increased with depth at location St3, decreased at St4 and were constant or increased at St5 and St6. In contrast, the M2 semi-major axes were almost constant over the entire measurement interval and equal to about 1 $\mathrm{cm\,s^{-1}}$. Hence, the amplification of the tidal signal near the shelf break concerns only the diurnal K1 tidal constituent and not the semi-diurnal (M2) one. Semi-minor axes are not plotted in the figure, but they were always smaller than 0.7 $\mathrm{cm\,s^{-1}}$ and 0.3 $\mathrm{cm\,s^{-1}}$ for K1 and M2, respectively. This means that the semi-minor axes were very small compared to the major ones and therefore tidal flow was almost rectilinear. The orientation of the semi-major axis was parallel to the isobaths, and it was roughly 60° at St3 and 80° at the other two stations, anticlockwise from east (trigonometric system).

5 Intensification of diurnal tide at the shelf-break and slope

As described in the previous sections, the diurnal tide (K1) presented a strong intensification during the summer-like (stratified water column) period (P2) at the shelf break (station St2). In addition, a weaker intensification just down-slope was observed at station St3 during the MATER and VECTOR periods. It seems that there was no similar manifestation at the inshore station St1 over the shelf. However, because of the measurement gaps it was not possible to compare the hourly flow at the two locations, St1

OSD
10, 435–472, 2013

and St2, for the same time period, but only for two periods similar as far as the density stratification is concerned, i.e. summers 1994 and 1995, as shown in Fig. 11. If we suppose that the summer 1994 circulation at location St1 is representative of the stratified conditions in general, it is evident from Fig. 10 that during summer the diurnal signal predominated only at location St2 (shelf edge). The cross-shelf u-component was of the same sign in the upper and in the bottom layers (Fig. 10a), even though the magnitude was different (larger at the bottom); the findings for the along-shelf v-component were similar (Fig. 10b). The current components at location St1 were totally different and occasionally of the opposite sign between the upper (depth 30 m) and the bottom layers (Fig. 10c and d).

Beckenbach and Terrill (2008) studied a similar diurnal phenomenon in the Southern California Bight, and they found that the structure of the diurnal internal tide resembled the vertical shape of the first baroclinic mode. The good vertical spatial resolution of their ADCP measurements enabled indication of such behaviour. In our case, the upper current meter at St2 was located at 56 m depth, therefore below the picnocline which during summer 1995 was located between 20 and 40 m depth (Fig. 11a). As shown in Fig. 11b, this depth is below the zero-crossing of the first baroclinic mode. Hence the values for the tidal amplitudes at the bottom current meter would be expected to be slightly greater than at the upper one and the signs should be the same, which is exactly what we observed.

The phenomena described in Beckenbach and Terrill (2008) happened in a situation with an abrupt bathymetric slope on the seaward side of the ridge. Their measurement site was poleward of the critical latitude for diurnal frequency internal waves, as was ours, and nevertheless currents were dominated by the diurnal signal. They explained this intensification in terms of a baroclinic internal tide generated through the interaction of a barotropic tide with topography. In these circumstances, subinertial internal waves can exist beyond the critical latitude and explain a consistent part of the variance. In particular, they observed an intensification of the across-shelf current component in accordance with the first baroclinic mode, with propagation of the signal from the shelf

OSD
10, 435–472, 2013

to the open sea. They also suggested the origin of the regularity of the amplified diurnal signal: excluding a possible effect of the sea breeze, its origin can be found either in the extension of the low limit in frequency of the internal wave spectrum when also including the horizontal component of the Coriolis parameter f, or in the presence of internal coastal-trapped waves. The first of these causes was excluded due to high stratification, that is, the Brunt-Väisälä stratification frequency $N \gg \Omega$ (rotation frequency), while the second one was considered possible, whether of remote and/or local origin.

In order to see whether any time dependence on a long-term scale can be demonstrated from our data, harmonic analysis was applied to 7-day-shifted, 30-day-long sub-samples, for the whole dataset. From this type of analysis it emerged (not shown here) that for the MATER dataset at St3 (the most complete in time coverage) and also for the bottom OTRANTO/OGEX dataset at St3 a slight intensification of the diurnal signal (up to almost $6\,\mathrm{cm\,s^{-1}}$ for the MATER series and up to almost $5\,\mathrm{cm\,s^{-1}}$ for the Otranto one) was found twice a year: in June–July and in December-January. This intensification, however, was quite weak (1–$2\,\mathrm{cm\,s^{-1}}$) with respect to the mean tidal diurnal semi-major axis value and it was not really significant. On the other hand, the semi-major axis at the bottom of location St2 had values between $15\,\mathrm{cm\,s^{-1}}$ and $20\,\mathrm{cm\,s^{-1}}$ until the end of July 1995, then decreased from the beginning of August through the subsequent months. The corresponding semi-minor axis values were also large, between $10\,\mathrm{cm\,s^{-1}}$ and $20\,\mathrm{cm\,s^{-1}}$, indicating a circular motion of the diurnal tide at this location. From the available data we saw that this intensification, however, appeared just once a year. Therefore the different behaviour at the two stations (St2 and St3) should be of different origin or at least a different manifestation of the same phenomena. Thus, for the purpose of better understanding the origin of the intensification, further analyses were performed with the bottom time-series at location St2 for the period May–November 1995.

Orlić et al. (2011) and Mihanović et al. (2009) found that summertime stratification occasionally generates internal coastal waves that travel daily around an island in the southern Adriatic Sea, creating the conditions for resonant excitation of the diurnal

OSD
10, 435–472, 2013

frequency by sea breeze and/or diurnal tides. In particular, Orlić et al. (2011) applied to the study zone the Princeton Ocean Model forced by real wind stress and found that an intensification of the diurnal signal, similar to that found in our data, is not possible without the topographic effect.

In the Otranto area the topography is a gently increasing slope from the coast to the position of the station St2; seaward from that location the bottom slope abruptly increases, reaching its maximum value between St2 and St3 (Fig. 1). The amplification of the diurnal signal in the currents at St2 is very prominent. As already pointed out, a weaker effect was also seen at St3, probably marginally influenced by the phenomenon. Moreover, temperature time-series measured at current-meter locations during the OTRANTO/OGEX project show spectra in which a weak diurnal peak was evident almost only at station St2, predominantly at the bottom, for period P2, and was practically absent in other periods and at the nearest stations (not shown). The stratification during summer was rather high (Fig. 11a) and, as for Beckenbach and Terrill (2008), this led us to exclude the possibility of the extension of the low-frequency limit of the internal spectrum.

In order to understand whether diurnal breeze can have some influence on the intensification, wind data were analysed by means of the Continuous Wavelet Transform. It performs a decomposition of the variability in time-scales (series), thus enabling establishment of correlations between series by comparing their respective wavelet power spectra on a scale-by-scale basis (Torrence and Compo, 1998; Torrence and Webster, 1999). As no on-shore station wind data were available for the year 1995, ECMWF (European Centre for Medium-range Weather Forecast) wind data at the grid point nearest to the St2 location were used. As it was not clear whether ECMWF data were able to resolve the diurnal signal, comparison with the on-shore station data (Otranto – 40.1471° N) for 2007 was performed and good agreement and resolution were found (not shown). Moreover, wavelet power spectra for both wind time-series during 2007 were calculated and similar levels of energy were found at diurnal frequency. ECMWF

OSD
10, 435–472, 2013

winds thus proved useful in trying to understand the importance of the diurnal signal and therefore they were used for discussing the 1995 phenomena.

Performing a wavelet analysis of the bottom current data at St2, the wind data and the sea level from the tide gauge located in Otranto (Rete Mareografica Nazionale, http://www.mareografico.it/) during summer 1995, interesting features emerged (Fig. 12). A strong diurnal signal with some modulation in time was seen in both current components, although it was more energetic for the u-component (cross-shelf). In general there was a weaker signal from the wind (relatively more pronounced in the cross-shelf u-component), occurring just occasionally. In contrast, sea level had a strong signal at the semi-diurnal frequency (modulated at 15 days) rather than at the diurnal one; this is in accordance with the characteristics of the Adriatic tides (Hendershott and Speranza 1971; Ursella and Gačić, 2001).

Multiple and partial coherences between wind, current and sea level on the diurnal scale have been calculated as in Mihanović et al. (2009). Multiple coherences were almost always above the 95 % confidence level, often very close to 1, while partial coherences between current components and wind components showed almost no values above the confidence level (Fig. 13). Finally, a wavelet spectrum was calculated for the off-shore station St3 and only a weak diurnal signal was found during period P2, while the coherence showed no correlation at all with wind data (not shown). This indicates that there was no wind influence on the diurnal scale of the current field.

We examined in more detail, but do not show here, the wind during summers 1994 and 1995: the breeze was present and it was more energetic during summer 1994 at St1 than during summer 1995. For this reason, any effect should be more evident in the 1994 current data. Moreover, its influence should be felt more strongly near the shore (St1) than further away (St2). However, the diurnal tide (K1 semi-major axis) at the near-shore station St1 in summer 1994 had values around 2.6–2.8 $\mathrm{cm\,s^{-1}}$. These are much smaller than at the bottom of St2 in summer 1995 (15 $\mathrm{cm\,s^{-1}}$) and similar to that found at the bottom of St3 in winter (4.2 $\mathrm{cm\,s^{-1}}$). Therefore no strong intensification

OSD
10, 435–472, 2013

of the diurnal signal was seen during summer 1994 near the coast and, accordingly, no correlation with the sea breeze was found.

Having excluded the effect of wind in the intensification of the diurnal tidal signal, the most probable cause remains the generation of internal waves that are coastally trapped by topography and resonate at the diurnal frequency. The presence of these internal diurnal waves was confirmed by the phase shift between the diurnal signal in the coastal sea level and in the currents at location St2 (Fig. 14a and b), and also from the lack of coherence between these two data sets (Fig. 13). However, these waves were not continuously generated (see wavelet spectra-Fig. 12), and did not generate amplification on the on-shore side of the shelf break (for example at station St1 in the similar stratification conditions of summer 1994). This indicates that the topographic slope as well as the density stratification is the necessary element for the resonance. Finally, we calculated the lagged cross-correlation between the sea level and the current at each level for the diurnal signal extracted by the wavelet analysis at station St2. The correlation functions show maxima shifted by one hour between the surface and bottom flow with respect to the sea level. (see Fig. 14c for the u-current component) with the one for the bottom preceding the upper-layer one. This indicates signal propagation from the bottom to the surface.

Finally, in order to possibly confirm the presence and propagation of this kind of internal tidal waves, VM-ADCP data were analyzed. As no data were available during the Otranto project, measurements for April 2007 were used. In fact, from the data we analysed (not shown here) it turns out that there was a weak stratification of the water column, even in April, and the described phenomena could possibly have taken place. Figure 15 shows that from transect 1 (TR1) to 3 (TR3) the cross-shore u-current component intensified while the signal propagated from the coastal area to the open sea, that is, during the rising tide in the sea level (Fig. 15c); the u-component then diminished again at transect 4 (TR4), i.e. during the falling diurnal tide in the sea level (Fig. 15c). The v-component (not shown) was dominated by the low-frequency signal

OSD
10, 435–472, 2013

with southward flow along the western coast and northward current along the eastern coast, obscuring any wave effect in this current component.

Is seems confirmed, therefore, that in the presence of stratification and the continental shelf-break, barotropic tide can generate internal waves that propagate seaward and are then amplified due to the resonance at the diurnal frequency.

6 Conclusions

We have analyzed some important features of the tidal flow at the transect in the Strait of Otranto using all available current-meter records from the period 1994–2007. Along the strait flanks the total variance was rather high, especially during the winter period, due to the generally strong meteorologically induced sub-tidal flow variability. Both tidal and low-frequency variances attained their minimum in the centre of the Strait of Otranto. However, in absolute terms the tidal flow, whose major contribution is represented by the diurnal (K1) constituent, reached its maximum at the channel flanks, in particular at the western continental shelf break. Moreover, the amplitude of the diurnal constituent showed annual variability, reaching a maximum in the stratified season. That the largest vertical amplitude of the diurnal constituent appeared in the deepest layer and increased towards the bottom is explained in terms of the first baroclinic mode pattern. We have excluded the possible sea-breeze impact on the intensification of the diurnal tidal signal and the most likely cause remains the generation of the topographically trapped internal waves and the diurnal resonance in the tidal response. These waves are sometimes generated by the barotropic tidal signal in the presence of density stratification. The effect was observed only in the vicinity of the topographic slope change. This phenomenon can stimulate both diapycnal mixing during the stratified season and sediment resuspension, and can enhance ventilation of the near bottom layers.

OSD
10, 435–472, 2013

Appendix A

Abbreviations

ADCP	Acoustic Doppler Current Profiler
CT	Conductivity-Temperature
CTD	Conductivity-Temperature-Depth
ECMWF	European Centre for Medium-range Weather Forecast
MATER	MAss Transfer and Ecosystem Response
MTP	Mediterranean Targeted Project
NWS	Normalized Wavelet Spectra
OGEX	Otranto Gap EXperiment
RDI	RD Instruments
VECTOR	VulnErabilità delle Coste e degli ecosistemi marini italiani ai cambiamenti climaTici e loro ruolO nei cicli del caRbonio mediterraneo
VM-ADCP	Vessel Mounted Acoustic Doppler Current Profiler

Acknowledgements. We greatly acknowledge the technical and scientific staffs of the OGS and of the former establishment SACLANTCEN of the Centre for Maritime Research and Experimentation (CMRE), Italy, as well as of the Hellenic Centre for Marine Research, Greece, who participated in the CTD, multi-beam and current meter data acquisition and pre-processing in the framework of the projects OTRANTO/OGEX, MATER and VECTOR. We are also grateful to the crew of the research vessels Urania, Aegeo, Alliance, ITS Magnaghi, OGS-Explora and Universitatis who helped in all the operations at sea. We are grateful to Vanessa Cardin for her help in extracting the ECMWF data. We appreciate the discussions on wavelet analysis and interpretation of results with Isaac Mancero Mosquera.

The central part of the bathymetry line used in Fig. 1c (~ 18.6–19.25° E) is a product of the multi-beam survey with high spatial resolution conducted on board r/v OGS-Explora in April 2007 (VECTOR).

OSD
10, 435–472, 2013

References

Beckenbach, E. and Terrill, E.: Internal tides over abrupt topography in the Southern California Bight: observations of diurnal waves poleward of the critical latitude, J. Geophys. Res., 113, C02001, doi:10.1029/2006JC003905, 2008.

Book, J. W., Martin, P. J., Janeković, I., Kuzmić, M., and Wimbush, M.: Vertical structure of bottom Ekman tidal flows: Observations, theory, and modeling from the northern Adriatic, J. Geophys. Res., 114, C01S06, doi:10.1029/2008JC004736, 2009.

Budillon, G., Grilli, F., Ortona, A., Russo, A., and Tramontin, M.: An assessment of surface dynamics observed offshore Ancona with HF radar, Marine Ecology PSZNI, 23, Supplement I, 21–37, 2002.

Buljan, M. and Zore-Armanda, M.: Oceanographical properties of the Adriatic Sea, Oceanogr. Mar. Biol. Ann. Rev., 14, 11–98, 1976.

Chavanne, C., Janeković, I., Flament, P., Poulain, P.-M., Kuzmić, M., and Gurgel, K.-W.: Tidal currents in the northwestern Adriatic: High Frequency radio observations and numerical model predictions, J. Geophys. Res., 112, C03S21, doi:10.1029/2006JC003523, 2007.

Cushman-Roisin, B., Malačič, V., and Gačić, M.: Tide, Seiches and Low-frequency oscillations, in: Physical Oceanography of the Adriatic Sea: Past, Present and Future, edited by: Cushman-Roisin, B., Gačić, M., Poulain, P.-M., and Artegiani, A., Kluwer Academic Publishers, Dordrecht/Boston/London, 217–240, 2001.

Cushman-Roisin, B. and Naimie, C. E.: A 3D finite-element model of the Adriatic tides, J. Mar. Syst., 37, 279–297, 2002.

Ferentinos, G. and Kastanos, N.: Water circulation patterns in the Otranto Strait, eastern Mediterranean, Cont. Shelf Res., 8, 1025–1041, 1988.

Foreman, M. G. G.: Manual for Tidal Currents Analysis and Prediction, Pacific Marine Science Report 78-6, Institute of Ocean Sciences, Patricia Bay, Sidney, BC, 57 pp. (2004 revision), 1978.

Gačić, M., Kovačević, V., Manca, B., Papageorgiou, E., Poulain, P.-M., Scarazzato, P., and Vetrano, A.: Thermohaline properties and circulation in the Strait of Otranto, in: Dynamics of Mediterranean Straits and Channels, edited by: Briand, F., Bull. Inst. Oceanogr., no. spécial 17, CIESM Science Series no. 2, Monaco, 117–145, 1996.

Hendershott, M. C. and Speranza, A.: Co-oscillating tides in long, narrow bays; the Taylor problem revisited, Deep-Sea Res., 18, 959–980, 1971.

OSD
10, 435–472, 2013

Janeković, I. and Kuzmić, M.: Numerical simulation of the Adriatic Sea principal tidal constituents, Ann. Geophys., 23, 3207–3218, doi:10.5194/angeo-23-3207-2005, 2005.
Janeković, I., Bobanović, J., and Kuzmić, M.: The Adriatic Sea M2 and K1 tides by 3D model and data assimilation, Estuar. Coast. Shelf Sci., 57, 873–885, 2003.
Kovačević, V., Gačić, M., and Poulain, P.-M.: Eulerian current measurements in the Strait of Otranto and in the Southern Adriatic, J. Mar. Syst., 20, 255–278, 1999.
Kovačević, V., Gačić, M., Mancero Mosquera, I., Mazzoldi, A., and Marinetti, S.: HF Radar Observations in the Northern Adriatic: Surface Current Field in Front of the Venetian Lagoon, J. Mar. Syst., 51, 95–122, 2004.
Leder, N., Smirčić, A., Ferenčak, M., and Vučak, Z.: Some results of current measurements in the area of the Otranto Strait, Acta Adriatica, 33, 3–16, 1992.
Lozano, C. J. and Candela, J.: The M2 tide in the Mediterranean Sea: dynamic analysis and data assimilation, Oceanol. Acta, 18, 419–441, 1995.
Malačič, V., Viezzoli, D., and Cushman-Roisin, B.: Tidal dynamics in the northern Adriatic Sea, J. Geophys. Res., 105, 26265–26280, doi:10.1029/2000JC900123, 2000.
Manca, B. B., Kovačević, V., Gačić, M., and Viezzoli, D.: Dense water formation in the Southern Adriatic Sea and spreading into the Ionian Sea in the period 1997–1999, J. Mar. Syst., 33–34, 133–154, 2002.
Martin, P. J., Book, J. W., Burrage, D. M., Rowley, C. D., and Tudor, M.: Comparison of model-simulated and observed currents in the Central Adriatic during DART, J. Geophys. Res., 114, C01S05, doi:10.1029/2008JC004842, 2009.
Michelato, A. and Kovačević, V.: Some dynamic features of the flow through the Otranto Strait, Boll. Oceanol. Teor. Appl., IX, 39–51, 1991.
Mihanović, H., Orlić, M., and Pasarić, Z.: Diurnal thermocline oscillations driven by tidal flow around an island in the Middle Adriatic, J. Mar. Syst., 78, S157–S168, doi:10.1016/j.jmarsys.2009.01.021, 2009.
Mosetti, F. and Manca, B.: Le maree dell'Adriatico: Calcoli di nuove costanti armoniche per alcuni porti. Studi in onore di Giuseppina Aliverti, Istituto Universitario Navale di Napoli, Ist. di Meteorologia e Oceanografia, 163–177, 1972.
Orlić, M.: Anatomy of sea level variability – an example from the Adriatic, in: The Ocean Engineering Handbook, edited by: El-Hawary, F., CRC Press, 1.1–1.14, 2001.

OSD
10, 435–472, 2013

Orlić, M., Beg Paklar G., Dadić, V., Leder N., Mihanović, H., Pasarić, M., and Pasarić, Z.: Diurnal upwelling resonantly driven by sea breezes around an Adriatic island, J. Geophys. Res., 116, C09025, doi:10.1029/2011JC006955, 2011.
Pawlowicz, R., Beardsley, B., and Lentz, S.: Classical tidal harmonic analysis including error estimates in MATLAB using T_TIDE, Comput. Geosci., 28, 929–937, 2002.
Polli, S.: La propagazione delle maree nell'Adriatico, Istituto Talassografico Sperimentale, Pubblicazione n. 370, Trieste, 11 pp, 1960.
Taylor, L.: Tidal oscillations in gulfs and rectangular basins, Proc. London Math. Soc., 20, 93–204, 1921.
Torrence, C. and Compo, G. P.: A practical Guide to Wavelet analysis, B. Am. Meteor. Soc., 79, 61–78, 1998.
Torrence, C. and Webster, P. J.: Interdecadal changes in the ENSO-monsoon System, J. Clim., 12, 2679–2690, 1999.
Ursella, L. and Gačić, M.: Use of the Acoustic Doppler Current Profiler (ADCP) in the study of the circulation of the Adriatic Sea, Ann. Geophys., 19, 1183–1193, doi:10.5194/angeo-19-1183-2001, 2001.
Ursella, L., Kovačević, V., and Gačić, M.: Footprints of mesoscale eddy passages in the Strait of Otranto (Adriatic Sea), J. Geophys. Res., 116, C04005, doi:10.1029/2010JC006633, 2011.
Ursella, L., Gačić, M., Kovačević, V., and Deponte, D.: Low-frequency flow in the bottom layer of the Strait of Otranto, Cont. Shelf Res., 44, 5–19, doi:10.1016/j.csr.2011.04.014, 2012.
Vetrano, A., Gačić, M., and Kovačević, V.: Water fluxes through the Strait of Otranto, in: EC Ecosystems research report No 32, The Adriatic Sea, Proceedings of the workshop "Physical and biogeochemical processes in the Adriatic Sea", Portonovo (Ancona), Italy, 23 to 27 April 1996, edited by: Hopkins, T. S., Artegiani, A., Cauwet, G., Degobbis, D., and Malej, A., 127–137, 1999.
Vilibić, I., Šepić, J., Dadić, V., and Mihanović, H.: Fortnightly oscillations observed in the Adriatic Sea, Ocean Dynam., 60, 57–63, doi:10.1007/s10236-009-0241-2, 2010.
Yari, S., Kovačević, V., Cardin, V., Gačić, M., and Bryden, H. L.: Direct estimate of water, heat, and salt transport through the Strait of Otranto, J. Geophys. Res., 117, C09009, doi:10.1029/2012JC007936, 2012.

OSD
10, 435–472, 2013

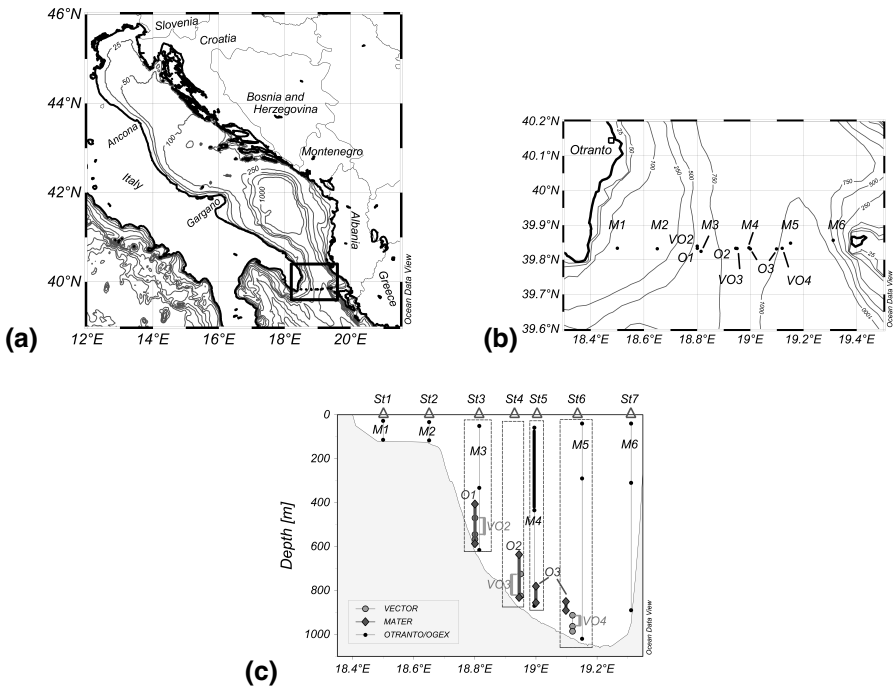

Fig. 1. (a) Study area in the Strait of Otranto at the southern end of the Adriatic Sea, depicted by a rectangle and expanded in **(b)**. **(b)** Mooring locations with original station nomenclature. Sea level and wind are available at the coast in Otranto. **(c)** Vertical scheme of the mooring lines: thick lines indicate layers covered by ADCPs. Both the original station nomenclature and the one adopted in this paper (St1, . . . , St7) are indicated. St3, St4, St5 and St6 enclose 2 or 3 moorings within dashed-line rectangles. Current measurements were conducted within the framework of different projects (see legend) during the time interval 1994-2007. Depth contours in **(a)** and **(b)** are in metres.

OSD
10, 435–472, 2013

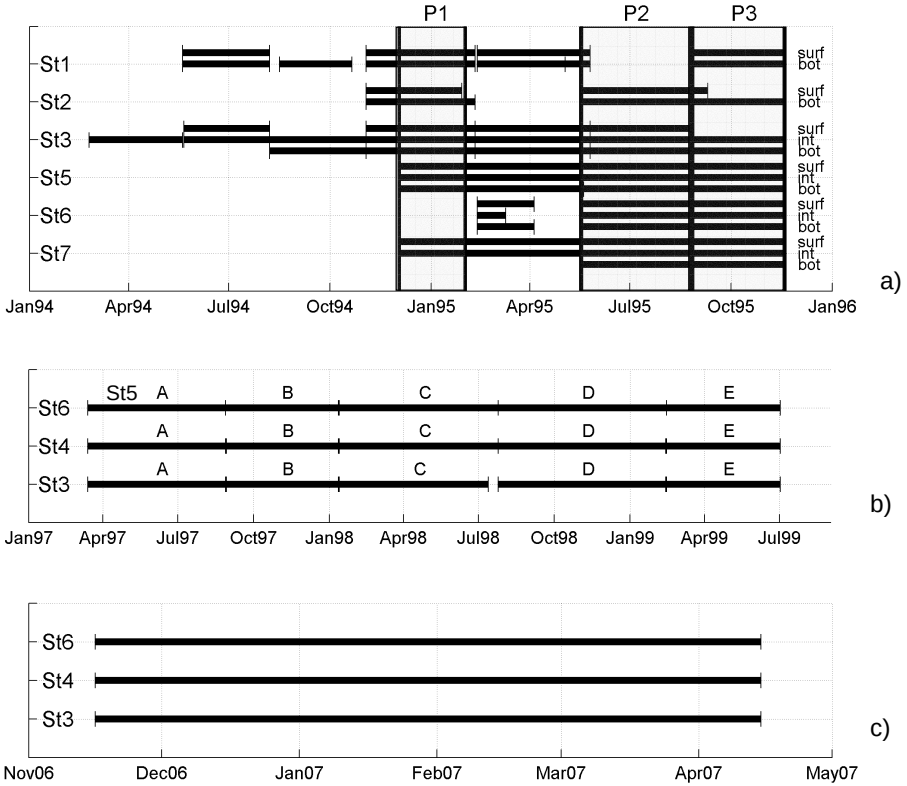

Fig. 2. Time diagram of the available current meter data within **(a)** the OTRANTO/OGEX project. Shaded areas correspond to time intervals for which rotary spectral analysis was done (P1, P2, and P3) **(b)** MATER project. Time intervals A, B, C, D and E are indicated. **(c)** VECTOR project.

OSD
10, 435–472, 2013

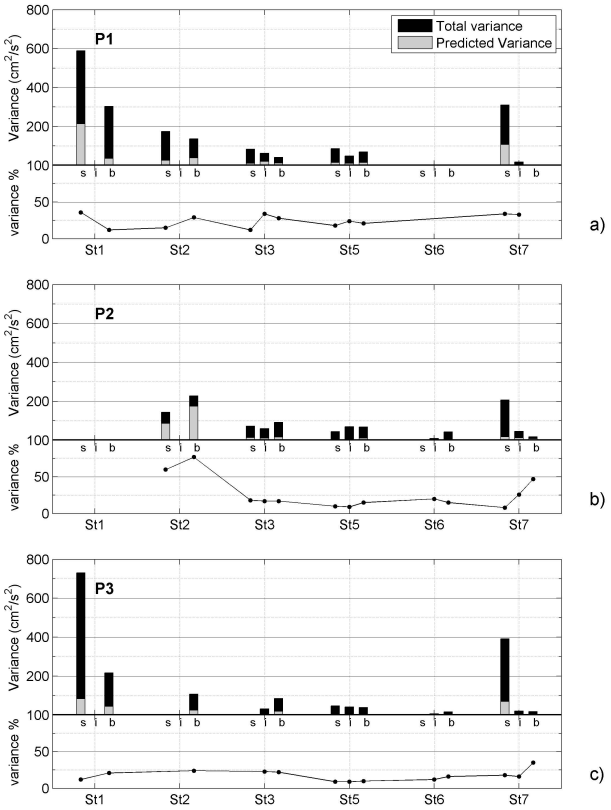

Fig. 3. Total variance (black bars) and predicted variance (grey bars), and the contribution of predicted to total (%; continuous line) due to all resolved tidal constituents (35) along the Otranto section, from OTRANTO/OGEX data for the three time intervals P1 **(a)**, P2 **(b)** and P3 **(c)**. Letters s, i, and b stand for surface, intermediate and bottom layers, respectively.

OSD
10, 435–472, 2013

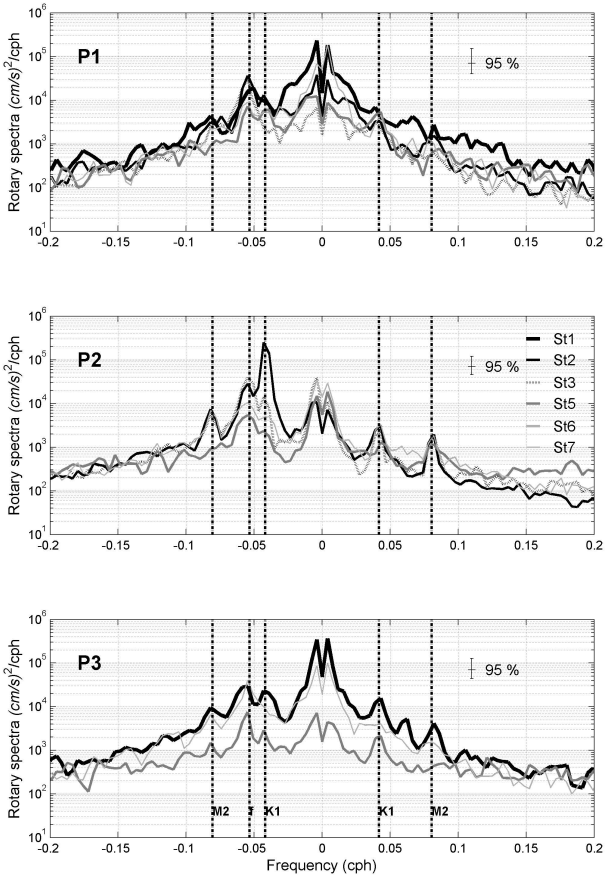

Fig. 4. Rotary spectral analysis in the upper layer along the Otranto section for the three time intervals P1, P2, and P3 from the OTRANTO/OGEX project. The 95 % confidence level is indicated.

OSD
10, 435–472, 2013

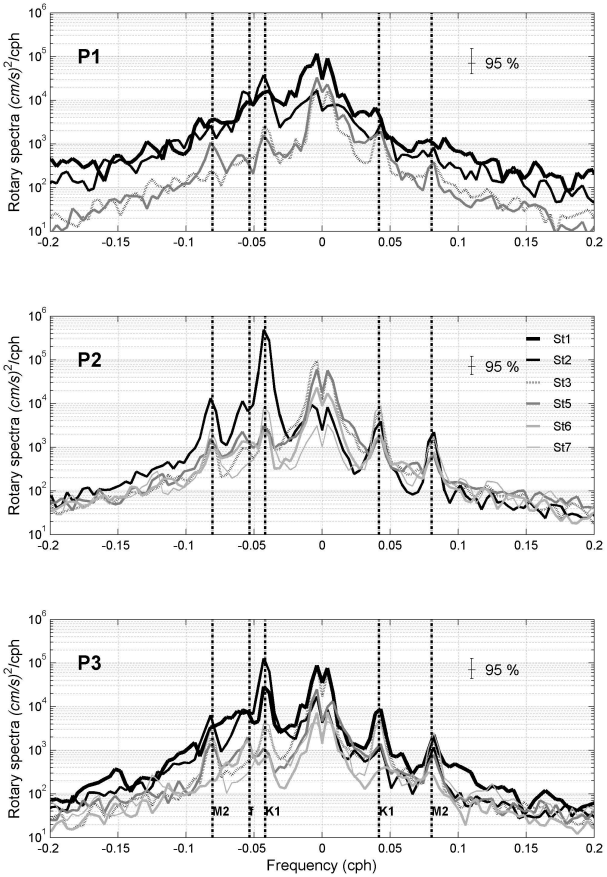

Fig. 5. Rotary spectral analysis in the near bottom layer along the Otranto section for the three time intervals P1, P2, and P3 from OTRANTO/OGEX project. The 95 % confidence level is indicated.

OSD
10, 435–472, 2013

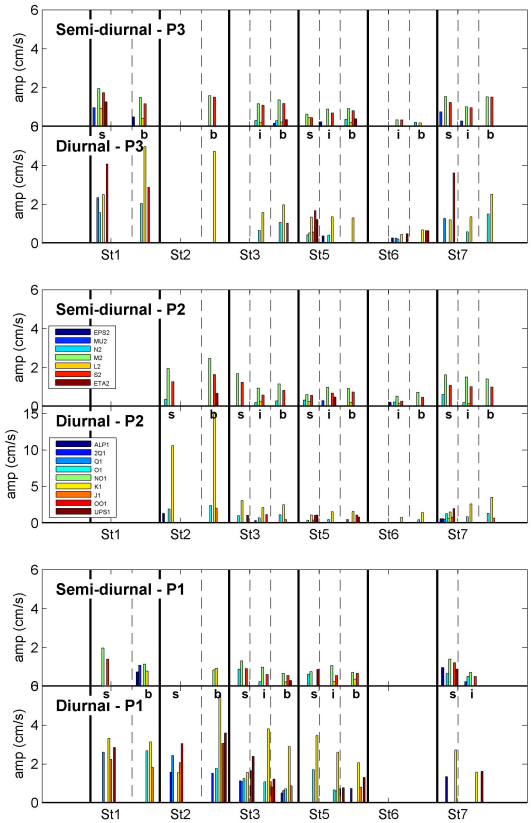

Fig. 6. Semi-major axes of the tidal ellipses for the diurnal and semi-diurnal tidal constituents, obtained from the harmonic analysis applied to the periods P1, P2 and P3 of the OTRANTO/OGEX project. Please note the different amplitude scale for the diurnal P2 plot. Letters s, i, and b stand for surface, intermediate and bottom layers, respectively.

OSD
10, 435–472, 2013

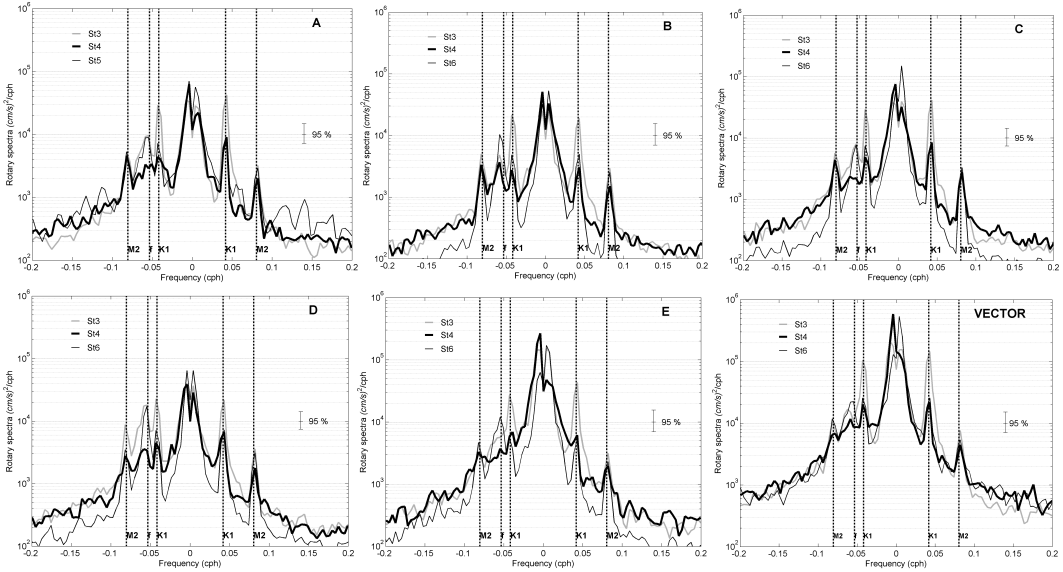

Fig. 7. Rotary spectra for the five MATER periods (A, B, C, D and E) and VECTOR. Inertial and principal tidal frequencies (M2 and K1) are indicated by dashed lines.

OSD
10, 435–472, 2013

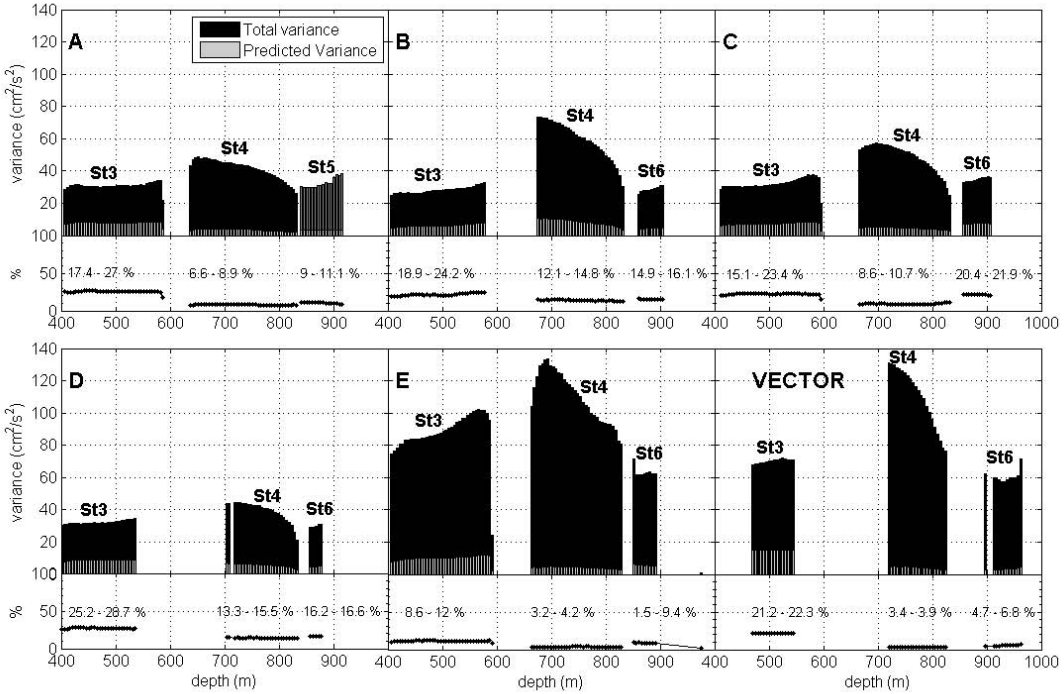

Fig. 8. Total variance (black bars), predicted variance (grey bars) and its contribution to the total one (%) as a function of depth. The predicted variance was calculated considering all the resolved tidal constituents (35) along the Otranto section, from MATER (periods A, B, C, D and E) and VECTOR data. Note that during period A, to avoid overlapping, the variances at St5 are plotted adding 60 m to the true depth.

OSD
10, 435–472, 2013

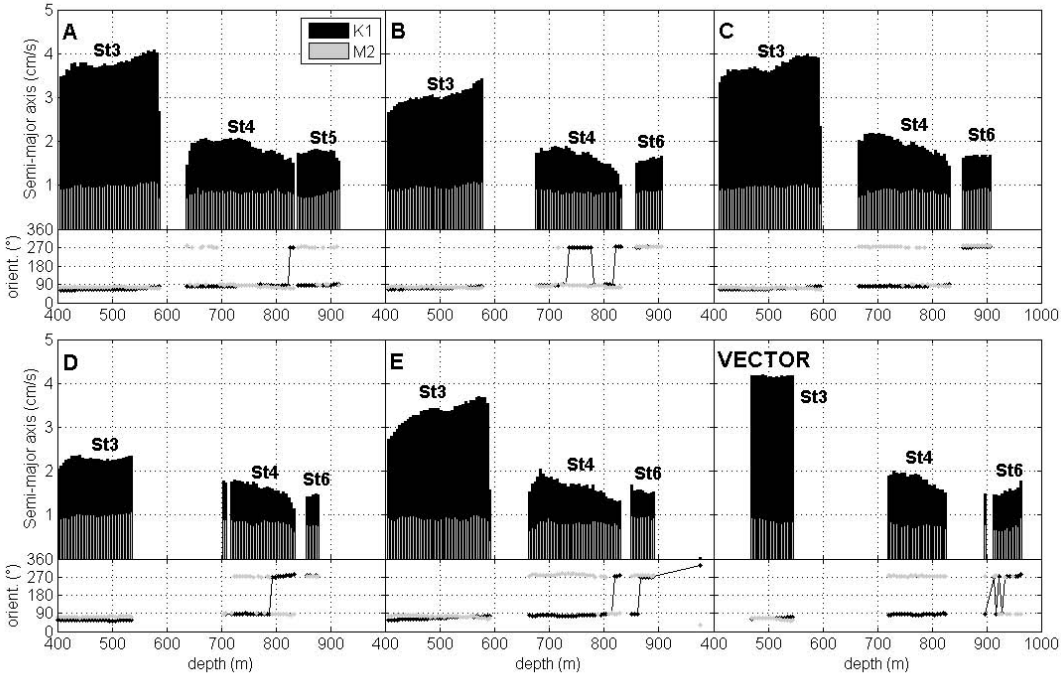

Fig. 9. Semi-major axes for K1 (black bars) and M2 (grey bars) with tidal ellipse orientation (in the trigonometric system) as a function of depth. The semi-axes were calculated with harmonic analysis for the bottom current meters along the Otranto section, from MATER (periods A, B, C, D and E) and VECTOR data. Note that during period A, to avoid overlapping, the semi-major axes at St5 are plotted adding 60 m to the true depth.

OSD
10, 435–472, 2013

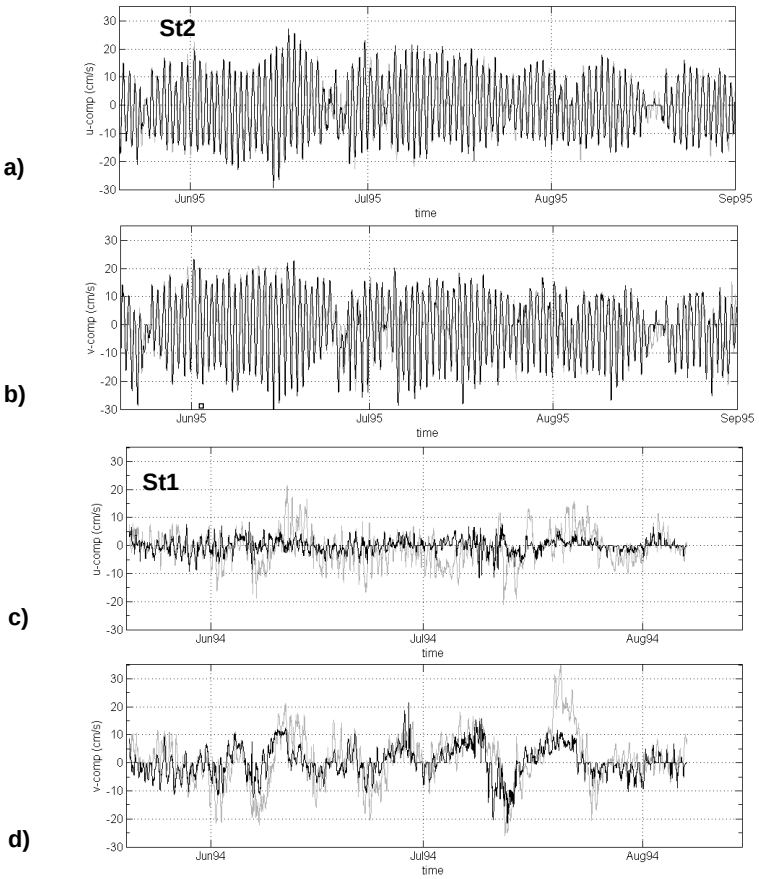

Fig. 10. U- and v-current components in the upper (grey line) and bottom (black line) layers at station St2 (**a** and **b**) during summer 1995 (P2) and at location St1 (**c** and **d**) during summer 1994.

OSD
10, 435–472, 2013

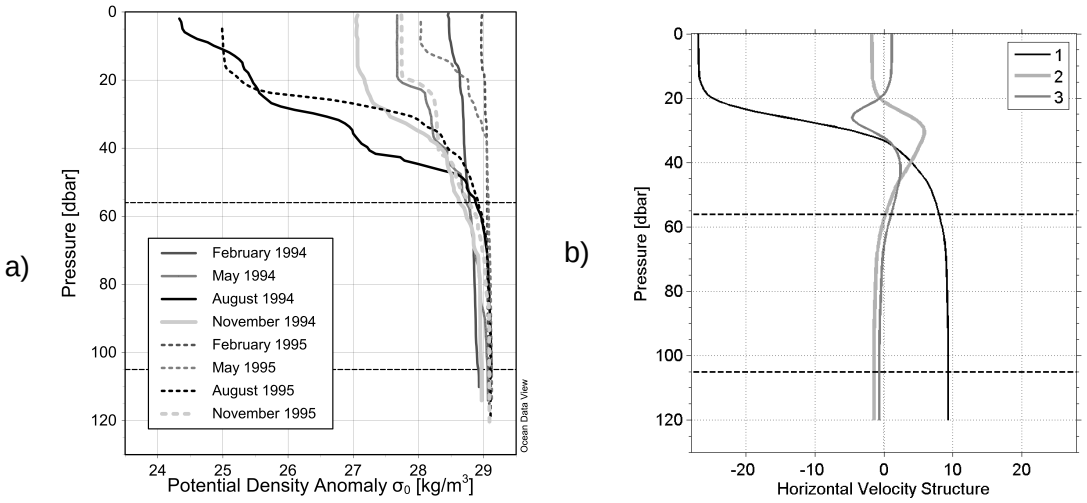

Fig. 11. (a) Potential density anomaly from the CTD surveys conducted in close proximity of St2 during OTRANTO/OGEX project. **(b)** Vertical distribution of the first three horizontal velocity modes at station St2 calculated from the August 1995 CTD profile. Current-meter depths at St2 are indicated by horizontal dashed lines.

OSD
10, 435–472, 2013

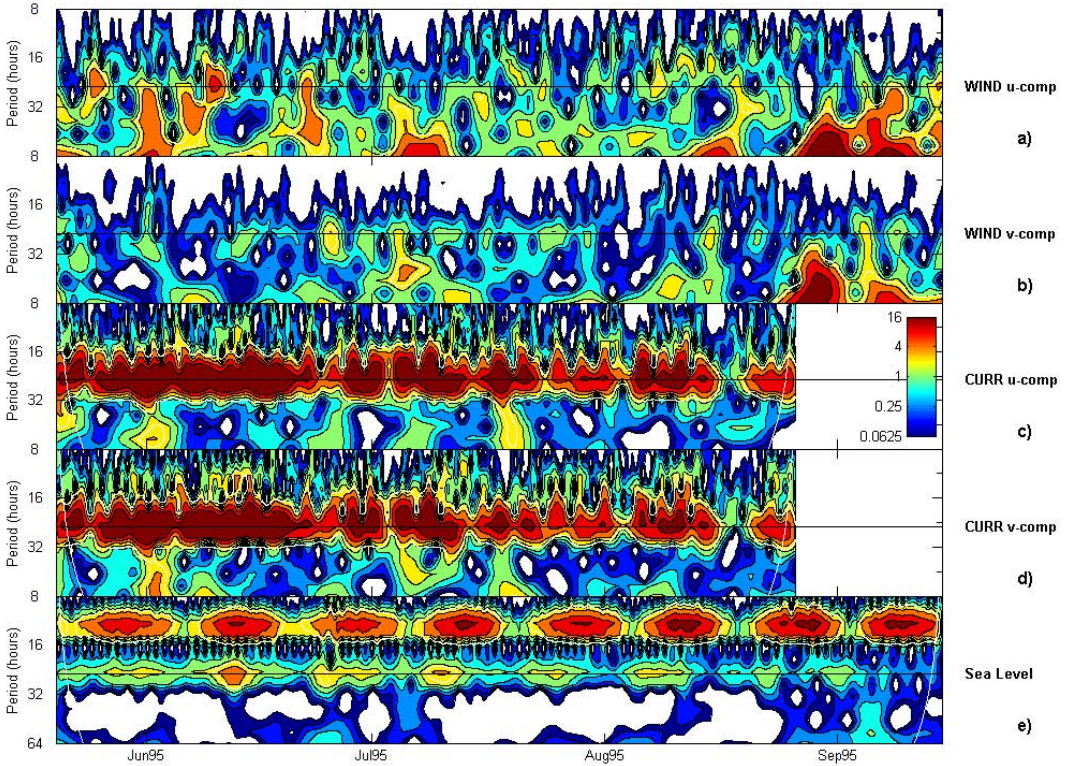

Fig. 12. Wavelet spectrum as a function of time and scale (period) for wind velocity components (**a** and **b**) and bottom current components (**c** and **d**) at St2, and sea level at Otranto **(e)** during period P2. Diurnal scale (24 h) is indicated by a black line.

OSD
10, 435–472, 2013

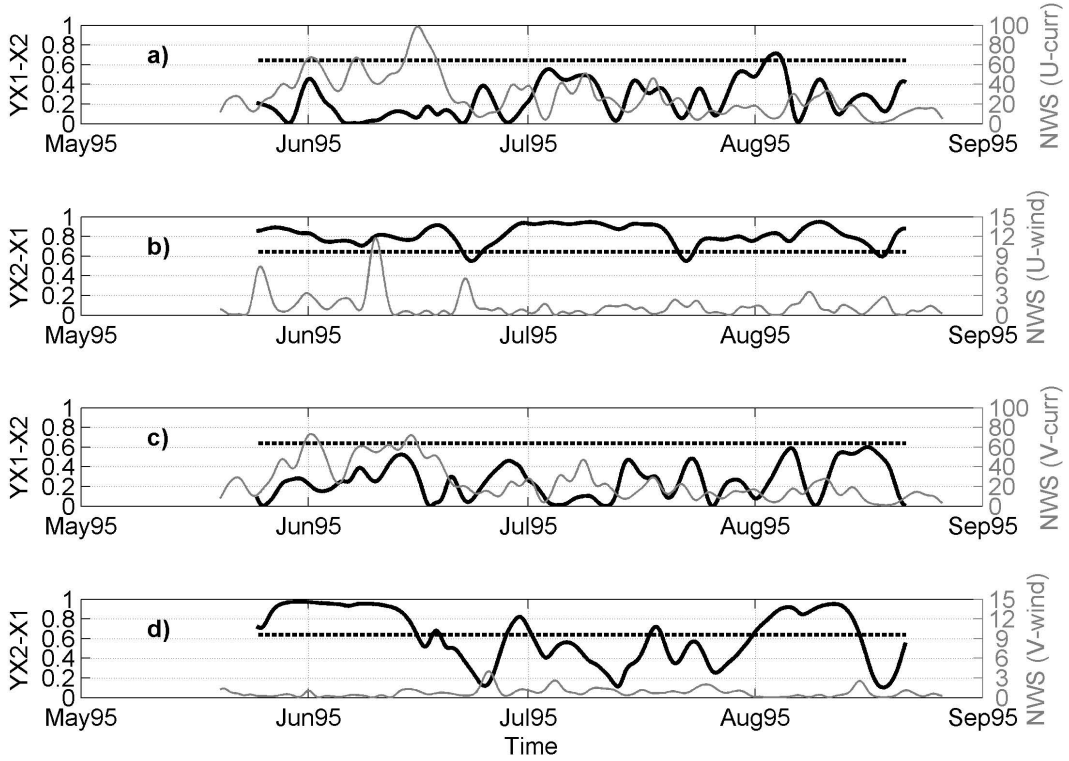

Fig. 13. Partial wavelet coherences squared (black line) and Normalized Wavelet Spectra (NWS; grey line) at St2 during summer 1995, at the diurnal band. Y is the current component, X1 is the wind component and X2 is the sea level at Otranto: u-component (**a** and **b**), v-component (**c** and **d**). The 95 % confidence level for partial wavelet coherences squared is indicated by the thick dashed line.

OSD
10, 435–472, 2013

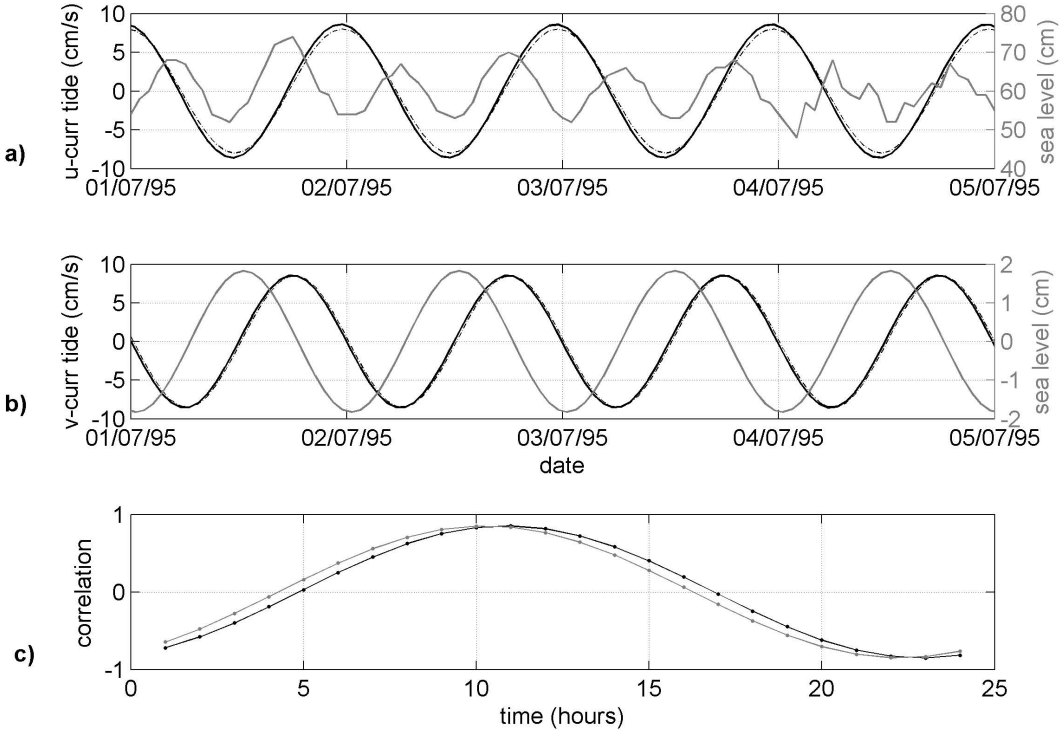

Fig. 14. Diurnal signal reconstructed from harmonic analysis for station St2, for the first four days of July 1995: **(a)** u-current component (black) and original sea level (grey); **(b)** v-current component (black) and diurnal signal in the sea level (grey). The upper and bottom current meters are indicated by solid and dash-dotted lines respectively. **(c)** 1-h lagged cross-correlation between the wavelet-extracted diurnal signal in the sea level and in the u-current component; the one for the upper layer is black while the one for the bottom is grey.

OSD
10, 435–472, 2013

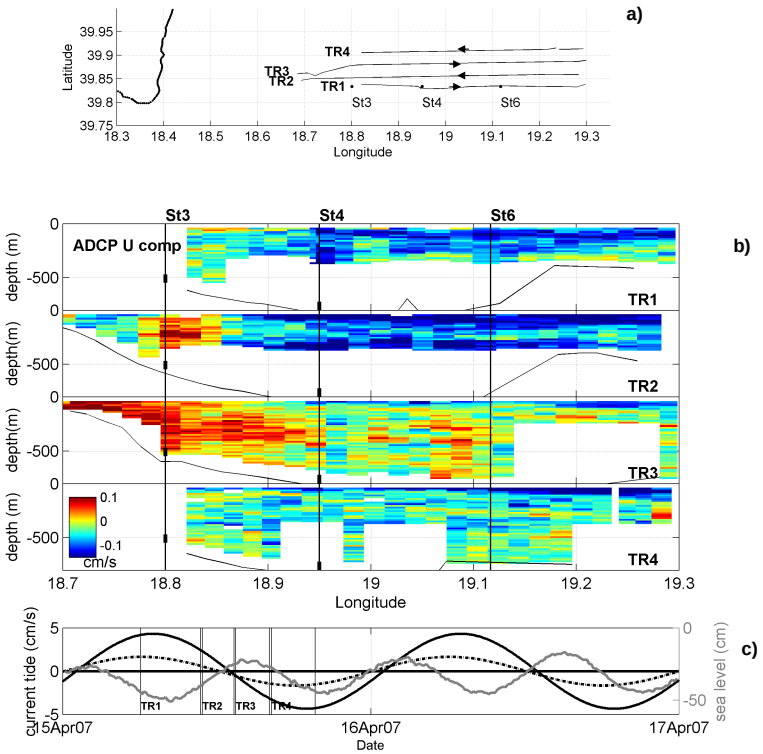

Fig. 15. U-current component **(b)** as measured by VM-ADCP along the sections indicated in the upper panel **(a)** and located in the Strait of Otranto during April 2007. Current-meter positions are indicated by dots in **(a)** and by thick lines in **(b)**. **(c)** Timing of different transects together with the diurnal current components (black lines) calculated from the deepest ADCP cell at St3, and sea level (grey line) from the Otranto on-land station; the u-component is plotted as a dash-dotted line while the v-component is the thick continuous line. The duration of transects is indicated by two vertical lines representing the start and end times.

OSD
10, 435–472, 2013